
Gradient-Matching Coresets for Rehearsal-Based Continual Learning

Lukas Balles¹

Giovanni Zappella¹

Cédric Archambeau¹

¹Amazon Web Services, Berlin

Abstract

The goal of continual learning (CL) is to efficiently update a machine learning model with new data without forgetting previously-learned knowledge. Most widely-used CL methods rely on a *rehearsal memory* of data points to be reused while training on new data. Curating such a rehearsal memory to maintain a small, informative subset of all the data seen so far is crucial to the success of these methods. We devise a coreset selection method for rehearsal-based continual learning. Our method is based on the idea of gradient matching: The gradients induced by the coreset should match, as closely as possible, those induced by the original training dataset. Inspired by the neural tangent kernel theory, we perform this gradient matching across the model’s initialization distribution, allowing us to extract a coreset without having to train the model first. We evaluate the method on a wide range of continual learning scenarios and demonstrate that it improves the performance of rehearsal-based CL methods compared to competing memory management strategies such as reservoir sampling.

1 INTRODUCTION

The incremental training of machine learning models on non-iid streams of data is a problem of great practical relevance. A recommender system may need to be updated with data from new categories of content or an object detection system may be confronted with new object categories or changes in lighting conditions or camera position. In such scenarios, we would like to efficiently update an ML model with new data without forgetting previously-learned knowledge.

Problems of this type recently received substantial interest from the ML community under the name of continual learn-

ing. While several specialized formulations of continual learning problems have been considered, we are interested in the most general one: We simply assume that we incrementally receive datasets $\mathcal{D}^{(1)}, \mathcal{D}^{(2)}, \dots$ without any guarantee of independence or stationarity. At time t , the goal is to have a model that performs well across all data seen so far, which we denote as $\mathcal{D}^{(1:t)}$. The individual datasets are referred to as “tasks” in more specialized formulations, such as class-incremental (new datasets contain previously-unseen classes) or domain-incremental (new datasets contain disjoint parts of the input space) scenarios. However, we also consider task-free scenarios, where the individual datasets do not necessarily correspond to conceptually distinct tasks.

With unlimited memory and computational resources, we might just store all datasets and retrain the model from scratch on $\mathcal{D}^{(1:t)}$. The challenge lies in getting close to this optimal performance while processing datasets incrementally, discarding one dataset (or most of it) before receiving the next. Naive approaches like simple incremental training on each incoming dataset lead to so-called *catastrophic forgetting*, the phenomenon of deteriorating performance on previously-observed data while training on new data.

Among the most widely-used and effective mechanisms to counteract forgetting is the use of a rehearsal memory of old data points to be reused while training on new data. Rehearsal-based methods are simple, robust, largely model-agnostic, and achieve state-of-the-art results [e.g., Buzzega et al., 2020]. Therefore, the curation of a rehearsal memory is a crucial aspect of continual learning.

In this paper we propose a simple and general coreset selection method for rehearsal-based continual learning. Our method is based on the idea of gradient matching: The gradients induced by the coreset should match, as closely as possible, those induced by the original dataset. Inspired by the neural tangent kernel theory, we perform this gradient matching across the model’s initialization distribution. This allows us to extract coresets without having to train the model and makes the method independent of the

model state and thereby compatible with most, if not all, rehearsal-based CL strategies. We demonstrate empirically that gradient-matching coresets improve the performance of rehearsal-based methods such as GDumb [Prabhu et al., 2020] and Experience Replay [Chaudhry et al., 2019] compared to other memory management strategies such as reservoir sampling or sliding window heuristics.

The paper is structured as follows. Our gradient-matching coreset method (GMC) is introduced in Section 2. Section 3 discusses some theoretical considerations, in particular the connection to the neural tangent kernel and an interpretation of GMC as *kernel mean matching*. Related work is discussed in Section 4. In Section 5 we evaluate the method experimentally on a diverse set of continual learning problems. We also provide a detailed sensitivity analysis with respect to the method’s hyperparameters. Finally, in Section 6 we conclude and suggest some future research directions.

2 GRADIENT-MATCHING CORESETS

We consider a supervised learning problem of predicting targets $y \in \mathcal{Y}$ from inputs $x \in \mathcal{X}$. We use a model $f(\cdot; \theta): \mathcal{X} \rightarrow \mathcal{Y}$ parametrized by $\theta \in \mathbb{R}^D$. While this could be any parametric model, we are mainly interested in neural networks. Given a loss function $l: \mathcal{Y} \times \mathcal{Y} \rightarrow \mathbb{R}$, any data point x, y induces a loss $\ell(\theta; x, y) = l(f(x; \theta), y)$. A training dataset $\mathcal{D} = \{(x_1, y_1), \dots, (x_N, y_N)\}$ implies a training loss

$$L_{\mathcal{D}}(\theta) = \frac{1}{N} \sum_{i=1}^N \ell(\theta; x_i, y_i). \quad (1)$$

During training, the model and the dataset interact via repeated evaluations of the gradient $\nabla L_{\mathcal{D}}(\theta)$. If we could select a subset $\mathcal{C} \subset \mathcal{D}$ such that $\nabla L_{\mathcal{C}}(\theta) \approx \nabla L_{\mathcal{D}}(\theta)$ for all “relevant” values of θ , we could hope to train the model on \mathcal{C} instead of \mathcal{D} with minimal loss in performance. Inspired by the neural tangent kernel theory [Jacot et al., 2018, Arora et al., 2019], we posit that the effect of the dataset on the model is, to a certain extent, characterized by the gradient across the initialization distribution, which we denote by $p(\theta)$. Therefore, we define the gradient matching error as

$$\mathbf{E}_{p(\theta)} \left[\|\nabla L_{\mathcal{C}}(\theta) - \nabla L_{\mathcal{D}}(\theta)\|^2 \right], \quad (2)$$

and seek to select a subset which minimizes this error.

We allow for a *weighted* subset and formalize the selection problem using a vector $w \in \mathbb{R}^N$ of weights and minimizing

$$\mathbf{E}_{p(\theta)} \left[\left\| \sum_{i=1}^N w_i \nabla \ell(\theta; x_i, y_i) - \sum_{i=1}^N \nabla \ell(\theta; x_i, y_i) \right\|^2 \right] \quad (3)$$

subject to a cardinality constraint $\|w\|_0 \leq n$, where $n \ll N$ is the desired coreset size and $\|w\|_0$ denotes the pseudonorm counting the non-zero entries in w .

The remainder of this section will be concerned with the efficient (approximate) solution of this problem. We make it tractable by constructing finite-dimensional embeddings of the per-data point gradient functions. The resulting cardinality-constrained quadratic problem may be solved approximately using greedy orthogonal matching pursuit [Mallat and Zhang, 1993], which we briefly review in Section 2.2. In Section 2.3, we devise a regularization scheme to avoid over-reliance on individual data points. The computational and memory cost of the method are discussed in Section 2.4. Finally, we adapt the algorithm to the continual setting in Section 2.5

2.1 GRADIENT EMBEDDINGS

As we cannot compute the expectation in Eq. (3) analytically, we approximate it by Monte Carlo integration:

$$\frac{1}{S} \sum_{s=1}^S \left\| \sum_{i=1}^N w_i \nabla \ell(\theta_s; x_i, y_i) - \sum_{i=1}^N \nabla \ell(\theta_s; x_i, y_i) \right\|^2, \quad (4)$$

where $\theta_1, \dots, \theta_S \sim p(\theta)$. We can write this compactly as

$$\min_{w \in \mathbb{R}^N} \|Gw - g\|_2^2 \quad \text{s.t.} \quad \|w\|_0 \leq n, \quad (5)$$

where we define the *gradient embedding* for the i -th data point as the concatenation of the gradients evaluated at all sampling locations,

$$g_i = \begin{bmatrix} \nabla \ell(\theta_1; x_i, y_i) \\ \vdots \\ \nabla \ell(\theta_S; x_i, y_i) \end{bmatrix} \in \mathbb{R}^{DS}, \quad (6)$$

as well as $G = [g_1 \ \dots \ g_N] \in \mathbb{R}^{DS \times N}$ and $g = \sum_{i=1}^N g_i \in \mathbb{R}^{DS}$. Eq. (5) is a cardinality-constrained quadratic problem, which is known to be NP-hard, but approximate solutions may be obtained with greedy methods.

Dimensionality reduction For large D and N , storing G becomes infeasible. To alleviate this issue, we project the individual gradients onto a lower-dimensional subspace using a projection matrix $P \in \mathbb{R}^{d \times D}$, i.e., we replace Eq. (6) with

$$g_i = \begin{bmatrix} P \nabla \ell(\theta_1; x_i, y_i) \\ \vdots \\ P \nabla \ell(\theta_S; x_i, y_i) \end{bmatrix} \in \mathbb{R}^{dS}. \quad (7)$$

We use sparse random projection matrices as proposed by Achlioptas [2001], see Appendix A for details. By construction, these projections satisfy $\mathbf{E}[P^T P] = I$ and thereby preserve inner products in expectation. Since our algorithm will rely entirely on inner products between gradient embeddings, this is a crucial property.

Last-layer variant As an additional means of reducing both the required memory and the computational cost of computing the gradient embeddings, we explored using only the gradients w.r.t. the last layer of the neural network model. These can be obtained at the cost of a forward pass through the network, see Appendix A. The last-layer gradient as a proxy for the full gradient has recently been used in work on active learning [Ash et al., 2020] and in the aforementioned concurrent work by Killamsetty et al. [2021].

2.2 ORTHOGONAL MATCHING PURSUIT

To approximately solve Eq. (5), we use a well-known greedy algorithm called orthogonal matching pursuit (OMP) [Mallat and Zhang, 1993], which we briefly outline here. In the context of OMP, the columns of G are referred to as dictionary elements and g is the target.

Assume we currently have a coreset, represented by an index set $I \subset [N]$ and corresponding weights $\gamma \in \mathbb{R}^{|I|}$. The coreset yields an approximation $g \approx G_I \gamma$, where G_I is the restriction of G to the columns contained in the index set I . Matching pursuit greedily adds the element which best matches the residual $r = g - G_I \gamma$. That is, we add $k_* = \arg \max_k g_k^T r$.

Orthogonal matching pursuit optimally readjusts the weights of all coreset elements after each greedy addition by solving $\min_{\gamma} \|G_I \gamma - g\|^2$. We stop the coreset construction when the desired size is reached. Algorithm 1 provides pseudo-code. In practice, OMP can be implemented more efficiently by incrementally updating the Cholesky decomposition of $G_I^T G_I$ as described in Appendix A.

Algorithm 1 Orthogonal Matching Pursuit

```

function OMP( $G = [g_1, \dots, g_N], g, n$ )
   $I \leftarrow ()$  ▷ Coreset indices
   $\gamma \leftarrow ()$  ▷ Coreset weights
  while  $|I| < n$  do
     $r = g - G_I \gamma$  ▷ Residual
     $k_* = \arg \max_{k \notin I} \langle g_k, r \rangle$ 
     $I \leftarrow I \cup \{k_*\}$ 
     $\gamma \leftarrow (G_I^T G_I)^{-1} G_I^T g$ 
  end while
  return  $I, \gamma$ 
end function

```

Of course, we would like the coreset weights to be nonnegative, since training on negatively-weighted examples would lead to catastrophic effects. While there are methods for nonnegative matching pursuit [e.g., Yaghoobi et al., 2015], they are more costly and complex to implement. Negative weights were not an issue in our experiments, especially in the presence of regularization (see below), so we do not explicitly enforce nonnegativity. As a safeguard, we manually clip the weights at zero in our implementation.

2.3 REGULARIZATION

In our application, we want to avoid over-reliance on individual data points in the form of outsize weights. This issue becomes particularly obvious if the desired coreset size approaches or even exceeds the embedding dimension dS , in which case any (linearly independent) subset will be able to match the target. It is tempting and straight-forward to add an Euclidan regularization term to the objective in Eq. (5). Indeed, this is done in related work [Killamsetty et al., 2021]. However, encouraging the weights to be small is, in some sense, misguided in our application. Instead, we want to encourage the weights to be close to “uniform”, i.e., to put roughly equal weight on all coreset elements.

To that end, we first identify the best uniform solution, $u_* = \arg \min_{u \in \mathbb{R}} \|G_I(u\mathbf{1}) - g\|^2$, where $\mathbf{1}$ denotes a vector of ones. Then, we set γ by minimizing

$$\|G_I \gamma - g\|_2^2 + \lambda \|\gamma - u_* \mathbf{1}\|_2^2 \quad (8)$$

As an added benefit, we are regularizing towards a *positive* weight for each coreset element.

To the best of our knowledge, such a regularization scheme has not been discussed in the literature on matching pursuit algorithms and might be of independent interest. We discuss in Appendix A how this regularization scheme can easily be integrated into efficient implementations of OMP.

2.4 COMPUTATIONAL AND MEMORY COST

Memory The memory required for the gradient embedding matrix G is $O(NSd)$. We use values for S in the range of 3–10 and $d = 1000$, making it feasible to store G even for large datasets. We also have to store the random projection matrix $P \in \mathbb{R}^{d \times D}$ but, owing to its sparsity (Appendix A), this requires only $O(\sqrt{D}d)$ memory. Finally, the individual parameter samples $\theta_1, \dots, \theta_S$ are of total size DS but could easily be stored on disk and loaded turn by turn when computing the gradient embeddings.

Compute The computational cost of obtaining the gradient embeddings is dominated by the cost of computing the gradients $\nabla \ell(\theta_s; x_i, y_i)$ for each sample $s = 1, \dots, S$ and data point $i = 1, \dots, N$. This corresponds to S epochs of training. We experimented with S in the range of 3–10, see also the sensitivity analysis presented in Section 5. Hence, the computational cost of obtaining the gradient embeddings is small compared to the cost of training the network on the full dataset, which typically takes dozens or hundreds of epochs. The last-layer variant further reduces the cost by eliminating the need for a full backward pass.

The computational cost of OMP is dominated by an $O(n^3)$ dependence on the desired coreset size [Rubinstein et al., 2008], which limits the scalability to very large coreset sizes.

In our experiments, we comfortably ran experiments up to $n = 10k$. In continual learning, it is usually desirable to keep the memory small.

2.5 CONTINUAL VERSION

Our main interest lies in continual learning, which is why we would like to apply GMC to a (non-iid) sequence of data batches, which need to be processed sequentially. For each incoming batch, we compute the corresponding gradient embedding matrix $G^{(t)} = [g_1^{(t)}, \dots, g_{N_t}^{(t)}] \in \mathbb{R}^{d_S \times N_t}$. The goal is to maintain a coreset which, after each new batch, matches the aggregate gradient of all data points seen so far, which we denote as

$$g^{(1:t)} := \sum_{s=1}^t \sum_{i=1}^{N_t} g_i^{(s)}. \quad (9)$$

Fortunately, our algorithm can be naturally extended to this setting. Let $C^{(t-1)}$ denote the gradient embedding matrix of the coreset after processing tasks 1 through $t-1$. Upon receiving $G^{(t)}$, we first update the target vector according to Eq. (9). We then run OMP with target $g^{(1:t)}$ and dictionary $G = [C^{(t-1)}, G^{(t)}]$. The gradient embedding matrix of the resulting coreset is stored for reuse in the next time step. Algorithm 2 provides pseudo-code.

Compared to an offline setting where $G^{(1)}, \dots, G^{(t)}$ are accessible simultaneously, we use the exact same target vector $g^{(1:t)}$ but a limited dictionary $[C^{(t-1)}, G^{(t)}]$ instead of $[G^{(1)}, \dots, G^{(t-1)}, G^{(t)}]$. Since $C^{(t-1)}$ is a coreset representative of $G^{(1)}, \dots, G^{(t-1)}$, we can expect the loss in performance to be small.

Note that the algorithm is free to remove and/or reweight elements from $C^{(t-1)}$, which allows it to flexibly react to new incoming data. When encountering data that is similar to data already in the coreset, we can compensate the change in the target vector by reweighting the existing coreset. When encountering novel data points, the algorithm will drop some coreset elements to free up capacity.

We want to emphasize that the algorithm extends so seamlessly to the continual setting because our gradient embeddings are based on the initialization distribution and therefore *constant*. This allows us to track the target vector (Eq. 9) exactly and to reuse the gradient embeddings for the coreset across time steps.

3 THEORETICAL CONNECTIONS

In this section we discuss two theoretical connections. First, we show that GMC is related to kernel mean matching w.r.t. a kernel defined via the inner product of gradients at initialization. Secondly, we discuss the connection of this kernel to the neural tangent kernel [NTK; Jacot et al., 2018, Arora et al., 2019].

Algorithm 2 Continual GMC

```

 $g \leftarrow 0$ 
 $C \leftarrow []$ 
while receiving  $\mathcal{D}^{(t)} = \{(x_1^{(t)}, y_1^{(t)}), \dots, (x_{N_t}^{(t)}, y_{N_t}^{(t)})\}$  do
     $G = \text{GRADIENT-EMBEDDING}(\mathcal{D}^{(t)})$ 
     $g \leftarrow g + \sum_i g_i^{(t)}$  ▷ Update target.
     $G \leftarrow [G, C]$  ▷ Combined dictionary.
     $I, \gamma = \text{OMP}(G, g, n)$ 
     $C \leftarrow G_I$ 
end while

```

3.1 GMC AS KERNEL MEAN MATCHING

Kernel associated with GMC For better readability, we introduce the shorthand $z = (x, y)$ for a labeled data point. We start by defining a kernel function between two data points as

$$k_{\text{GMC}}(z, z') := \mathbf{E}_{p(\theta)}[\nabla \ell(\theta; z)^T \nabla \ell(\theta; z')]. \quad (10)$$

That is, the inner product of the two data points' gradients, averaged over the initialization distribution $p(\theta)$. The implicit feature function ϕ underlying this kernel maps a data point $z = (x, y)$ to its associated gradient function, $\phi(z) = \nabla \ell(\cdot; z) \in \mathcal{G}$ living in the space \mathcal{G} of functions $\mathbb{R}^D \rightarrow \mathbb{R}^D$. If we equip this space with the inner product $\langle g, g' \rangle_{\mathcal{G}} = \mathbf{E}_{p(\theta)}[g(\theta)^T g'(\theta)]$, we recover the kernel via $k_{\text{GMC}}(z, z') = \langle \phi(z), \phi(z') \rangle_{\mathcal{G}}$. Using this notation, our gradient matching objective from Eq. (3) can be written as

$$\left\| \sum_{i=1}^N w_i \phi(z_i) - \sum_{i=1}^N \phi(z_i) \right\|_{\mathcal{G}}^2, \quad (11)$$

which we minimize under a cardinality constraint on w .

The object $\frac{1}{N} \sum_i \phi(z_i)$ is the (empirical) kernel mean embedding of the data distribution w.r.t. the kernel associated with ϕ . Kernel mean embeddings [Smola et al., 2007] represent a distribution in a reproducing kernel Hilbert space and can be used for a variety of tasks, e.g., measuring distances between distributions or performing two-sample tests.

Kernel mean matching One use of kernel mean embeddings, which is related to our application, is kernel mean matching [Huang et al., 2006]. Assume we have a kernel $k(x, x')$ operating on inputs x . Denote the corresponding feature map as $\psi(x)$ which maps to some Hilbert space \mathcal{H} . Also assume that you have two data samples x_1, \dots, x_N and $x'_1, \dots, x'_{N'}$, generated by $p(x)$ and $p'(x')$, respectively. Kernel mean matching finds weights w which minimize

$$\left\| \frac{1}{N} \sum_{i=1}^N w_i \psi(x_i) - \frac{1}{N'} \sum_{i=1}^{N'} \psi(x'_i) \right\|_{\mathcal{H}}^2 \quad (12)$$

subject to the constraint $w_i \geq 0$. In other words, we reweight the samples from $p(x)$ such as to better match the kernel mean embedding of $p'(x)$, akin to importance sampling. A typical application is to correct for a sample selection bias.

Comparison Comparing Eqs. (11) and (12), GMC can be seen as a form of kernel mean matching where the source and target distributions are *identical* and we impose a cardinality constraint. Note, however, that we use a kernel and associated feature function that operates on labeled data points $z = (x, y)$, whereas existing applications of kernel mean matching use kernels operating on inputs only.

3.2 RELATIONSHIP TO THE NTK

Recall that $\ell(\theta; x, y) = l(f(x; \theta), y)$, where $f(\cdot; \theta): \mathcal{X} \rightarrow \mathcal{Y}$ denotes the forward map of the neural network and $l: \mathcal{Y} \times \mathcal{Y} \rightarrow \mathbb{R}$ is the loss function. The neural tangent kernel is defined for a regression problem—i.e., $\mathcal{Y} = \mathbb{R}$ and $l(\hat{y}, y) = \frac{1}{2}(\hat{y} - y)^2$ —and reads

$$k_{\text{NTK}}(x, x') = \nabla_{\theta} f(x; \theta)^T \nabla_{\theta} f(x'; \theta), \quad (13)$$

evaluated at a location $\theta \sim p(\theta)$ sampled randomly from the initialization distribution.

The two gradients featuring in Eq. (10) and Eq. (13) are closely related, since

$$\nabla \ell(\theta; x, y) = l'(f(x; \theta), y) \nabla_{\theta} f(x; \theta). \quad (14)$$

However, there are two key differences between the NTK and the GMC kernel. First, the NTK operates on inputs x , whereas the GMC kernel operates on input-output pairs (x, y) . Second, while the GMC kernel is averaged over $p(\theta)$, the NTK is evaluated at a single location sampled randomly from $p(\theta)$. The theory associated with the neural tangent kernel is concerned with the so-called infinite-width limit, where the number of units in each layer of the neural network grows to infinity. While the kernel defined in Eq. (13) depends on the (randomly-sampled) θ for a finite-width model, it converges to a deterministic object in the infinite-width limit.

4 RELATED WORK

Continual learning has received significant attention in recent years. Several approaches to counteract forgetting have been explored, such as regularization [Kirkpatrick et al., 2017, Zenke et al., 2017], dynamically evolving architectures [Rusu et al., 2016, Mallya and Lazebnik, 2018, Serra et al., 2018], or knowledge distillation [Li and Hoiem, 2017, Rebuffi et al., 2017].

Among the most widely-used methods are those that rely on a so-called *rehearsal memory* [Robins, 1995] of data

points to be reused while training on new data. Rehearsal-based methods are simple, robust, and largely agnostic to the model class. A simple but effective method in this family is *Experience Replay* [Robins, 1995, Chaudhry et al., 2019], which trains jointly on the current task data and the memory. Different memory curation strategies can be used but reservoir sampling [Vitter, 1985], which maintains a uniform random subsample from a stream of data points, has been found to work best by Chaudhry et al. [2019]. Other works have relied on sliding window heuristics, e.g., Lopez-Paz and Ranzato [2017]. In a notable paper, Prabhu et al. [2020] demonstrated that retraining—from scratch—on a greedy class-balanced memory alone is competitive with a number of more complex methods; a finding which underscores the significance of a rehearsal memory.

A number of works provide solutions for curating a rehearsal memory in a more informed manner. We limit the discussion to the methods most relevant to the present work. Aljundi et al. [2019] propose gradient-based sample selection (GSS), which assembles a set of data points with diverse gradients by minimizing the sum of their pairwise cosine similarities. Yoon et al. [2021] seek to maximize a combination of gradient diversity and gradient similarity to the current task. Borsos et al. [2020] construct coresets for continual learning using a bilevel optimization approach which also relies on matching pursuit.

Outside of continual learning, Campbell and Broderick [2018] use a similar technique to select coresets for efficient Bayesian inference with Monte-Carlo methods. Zhao et al. [2020] use a related notion of gradient matching to construct *synthetic* datasets.

Recent independent work by Killamsetty et al. [2021] is closely related to our method, but pursues a different goal, namely to reduce the computational cost of training a model in an offline (non-continual) setting. They use gradient matching to select an “active set” of points, which are used to train the model for a small number of epochs, after which the selection is repeated. Their method is based on gradients evaluated *locally* at the current location in parameter space. Since the whole dataset has to be retained for the repeated coreset selection, their method is not directly applicable to continual learning. We experimented with a “local version” of our algorithm (see Appendix A), which can be seen as an adaptation of the method of Killamsetty et al. [2021] to the continual setting.

5 EXPERIMENTS

We evaluate the performance of GMC against different memory curation strategies for continual learning. While GMC may be used with any rehearsal-based CL method, for the purpose of this comparison we leverage two simple and well-know algorithms: a variant of GDumb [Prabhu et al.,

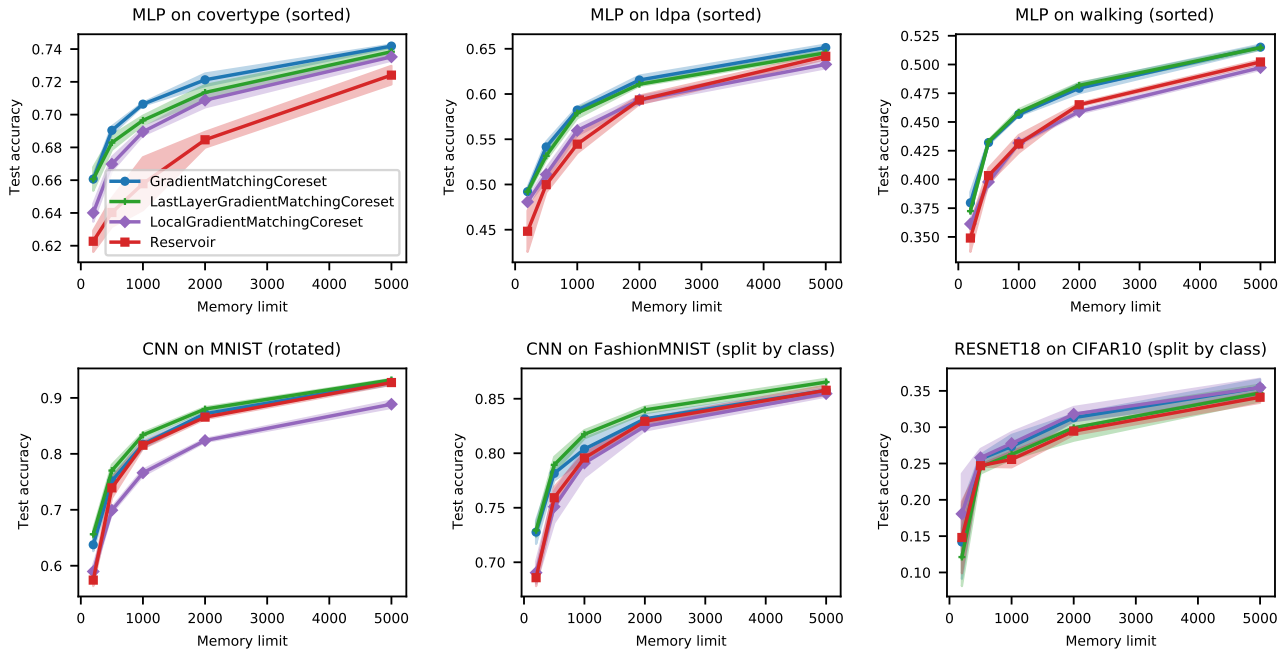


Figure 1: Experimental results for different memory curation strategies in the GDumb paradigm. The graphs depict the final test accuracy, after seeing all tasks/batches, as a function of the memory size. Results are averaged over five random seeds and the shaded area spans one standard deviation.

2020] and Experience Replay [Chaudhry et al., 2019].

5.1 EXPERIMENTAL SETUP

CL Methods Upon receiving a new batch of data, GDumb updates its rehearsal memory, reinitializes the model and trains it from scratch using only the data in memory. The rehearsal memory is the *sole* mechanism counteracting forgetting, and therefore these experiments clearly isolate the effect of the memory curation strategy. While Prabhu et al. [2020] use a greedy class-balancing memory, we use the same approach with other memory curation strategies.

In Experience Replay, we train on the union of the current task data and the memory. The model is trained continually without reinitializing. The memory is updated when training for a task has terminated.

Benchmarks We present experiments training an MLP on three tabular datasets, COVERTYPE, LDPA, and WALKING ACTIVITY, from OpenML [Vanschoren et al., 2013], a CNN on MNIST [LeCun and Cortes, 2010] and FASHION-MNIST [Xiao et al., 2017], as well as a ResNet-18 [He et al., 2016] on CIFAR10 [Krizhevsky et al., 2009]. To demonstrate the versatility of the method, we use a wide variety of continual learning scenarios. For the tabular datasets, we generate a challenging task-free scenario by sorting the data points according to the value of a single feature and splitting into 10 equally sized batches. There is no notion of distinct tasks

but a continuous drift in the input distribution. For MNIST, we follow Lopez-Paz and Ranzato [2017] and generate a domain-incremental scenario by splitting the dataset into 4 folds and rotating the images by 0, 90, 180, and 270 degrees, respectively. For FASHION-MNIST and CIFAR-10, we use the popular class-incremental scenario, where the dataset is divided into discrete tasks, each consisting of two classes. Full experimental details may be found in Appendix B.

Baselines We compare GMC to Reservoir Sampling [Vitter, 1985], the greedy class-balancing method used by [Prabhu et al., 2020], a simple sliding window heuristic, as well as the gradient-based sample selection (GSS) strategy of Aljundi et al. [2019]. Lastly, we experimented with a “local” variant of GMC, which may be seen as a continual version of the method of Killamsetty et al. [2021]. Details are explained in Appendix A, but the basic idea is to perform gradient matching *locally*, at the current location in parameter space. All competitors have been tested using memories of 200, 500, 1000, 2000 and 5000 data points.

Hyperparameters We used a fixed hyperparameter setting for GMC across all experiments, identified with a few exploratory experiments. To compute the gradient embeddings, we used $S = 10$ draws from the initialization distribution and a projection dimension of $d = 1000$. The sensitivity analysis in Fig. 3 suggests that these are generous values and could likely be reduced without sacrificing performance. We use a regularization coefficient of $\lambda = 0.5$.

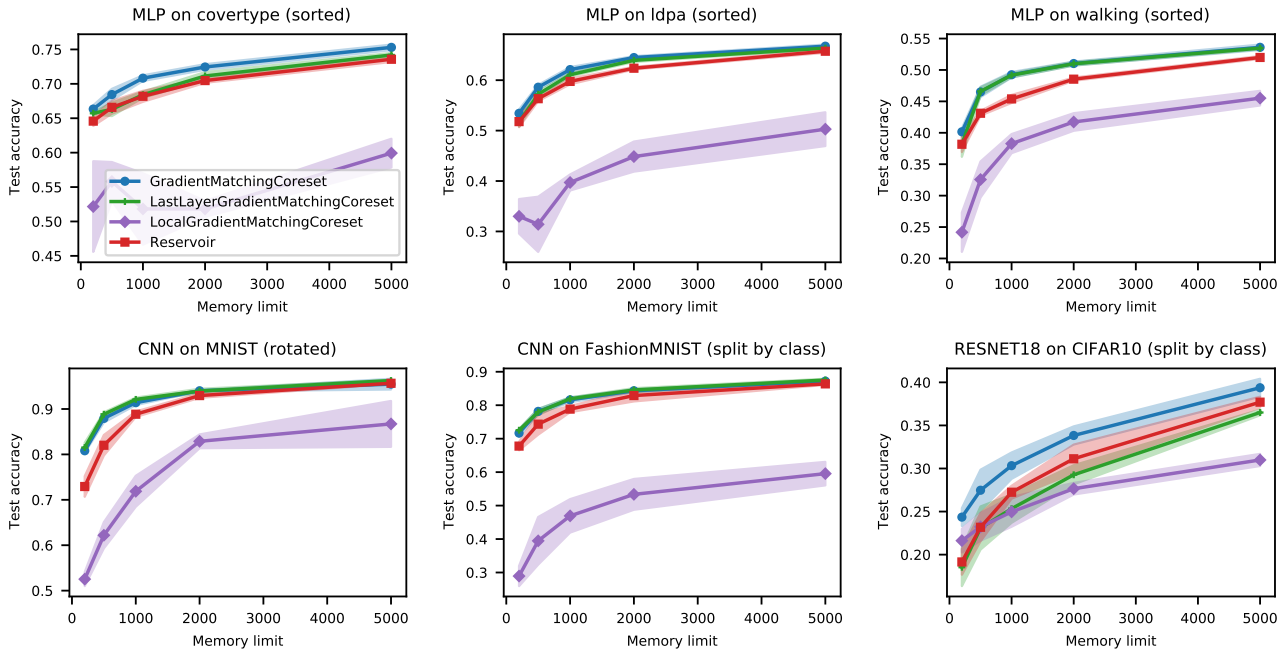


Figure 2: Experimental results for different memory curation strategies in the Experience Replay paradigm. The graphs depict the final accuracy, after seeing all tasks/batches, on the full test set as a function of the memory size. Results are averaged over five random seeds and the shaded area spans one standard deviation.

Regarding the optimization procedure, we opted for a single set of hyperparameters across all experiments. We used the Adam optimizer [Kingma and Ba, 2014] with a constant step size of $3 \cdot 10^{-4}$ and other hyperparameters set to default values. We employed a weight decay penalty of 10^{-4} and used a minibatch size of 100. These settings are not tuned to the individual problems and therefore likely suboptimal, but we prioritized a clean and simple comparison between the memory curation strategies over state-of-the-art results.

5.2 RESULTS

Due to space constraints, full results for all memory curation strategies are reported in Tables 1 and 2 in the Appendix. Here, in Figures 1 and 2, we visualize the comparison between GMC (in its different versions) and Reservoir Sampling, which proved to be the strongest competitor, in line with findings by Chaudhry et al. [2019]. We see that GMC achieves consistent improvements over Reservoir Sampling and the other baselines in all scenarios and across all tested memory sizes, both in GDumb and Experience Replay. The size of the effect varies and tends to be larger at small memory sizes. It is quite substantial in the tabular datasets, e.g., on COVERTYPE with a memory size of 1000, GMC boosts the test accuracy to roughly 70% compared to the 65% achievable with Reservoir Sampling, a relative increase of 7.7%. The increase in performance is more modest in the vision experiments, but still considerable for small memory sizes, especially in the ER experiments. In any case, GMC

never underperforms Reservoir Sampling.

As can be seen in the Tables 1 and 2, the greedy class-balancing method used in the original GDumb paper matches Reservoir Sampling in the class-incremental scenarios, but fails in the task-free and domain-incremental scenarios, where there is a continual dynamic beyond a shift in class occurrences. The sliding window heuristic performs poorly across the board.

The last-layer variant of GMC matches the performance of the full variant in most experiments and even performs *better* in a few cases. However, there is the notable exception of the ResNet experiment, where it underperforms especially when using Experience Replay. One might conjecture that the last layer gradient is a poor proxy when using such deep architectures.

The local version—a naive adaptation of the method of Killamsetty et al. [2021] to the continual setting—has mixed performance. Somewhat surprisingly, it performs decently in some GDumb experiments, but drastically underperforms when used with ER. We conjecture that the gradients at a single point in parameter space are not informative enough to select coresets that are useful beyond a small number of training epochs. See also our sensitivity analysis regarding the number of samples S .

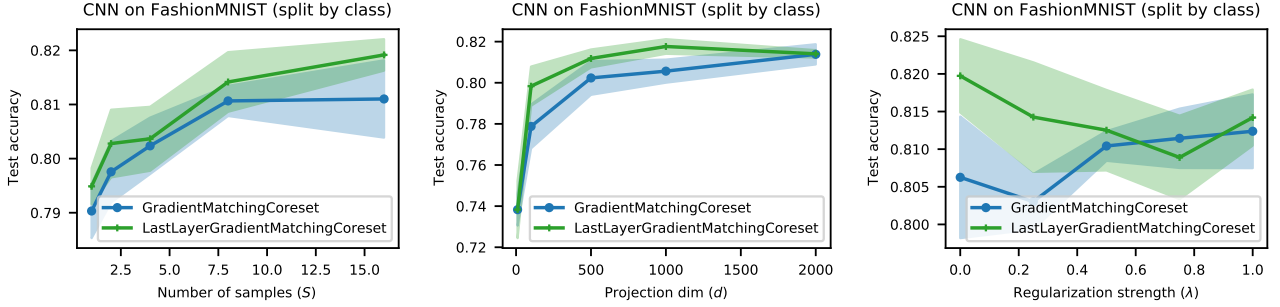


Figure 3: Hyperparameter sensitivity of GMC.

5.3 ABLATION STUDIES

GMC exposes three hyperparameters: The number of samples from the initialization distribution (S), the projection dimension (d) and the regularization strength (λ). We ran a (univariate) sensitivity analysis with respect to these hyperparameters on the FASHION-MNIST experiment in the GDumb setting at a memory size of 1000. The results are depicted in Figure 3. For the gradient embedding parameters (S and d) we see, as expected, an increasing trend but the effect seems to saturate quite quickly. For the projection dimension, any value larger than 500 seems to work almost equally well. The performance seems to be relatively insensitive to the choice of the regularization strength (λ) in this particular experiment. However, we can anecdotally report that adding some regularization improves the robustness of the algorithm.

We also investigated the sensitivity to the choice of the initialization distribution $p(\theta)$. In all experiments above, we used the default initialization scheme implemented in PyTorch (`kaiming_uniform`), which is the uniform version of the scheme proposed by He et al. [2015]. In Figure 4, we compare this default scheme to the corresponding normal (Gaussian) version (`kaiming_normal`). We vary the scale of these distributions by multiplying the random draws by a scale parameter. These experiments were run on the FASHION-MNIST problem using GDumb with a fixed memory size of 1000. The performance of GMC is remarkably insensitive to these variations of the initialization distribution.

6 CONCLUSION

We introduced the Gradient-Matching Coreset method (GMC). Our method is simple, robust and scales to coreset sizes of several thousand data points. It naturally extends to the continual learning setting, where it can be used to curate a memory for any rehearsal-based strategy. We empirically evaluated its performance on a variety of continual learning scenarios including tabular and image data, bal-

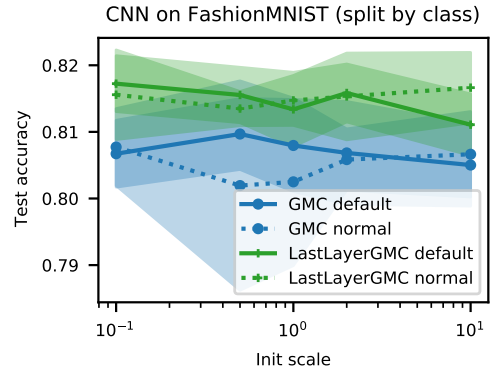


Figure 4: Sensitivity to the type and scale of the initialization distribution.

anced and imbalanced datasets, as well as different types of continual learning scenarios (class-incremental, domain-incremental, task-free). GMC is never worse than and often outperforms its strongest competitor, Reservoir Sampling, across all memory sizes.

There are several avenues for future work. It would be interesting to explore the use of GMC with more advanced rehearsal-based methods such as Dark Experience Replay [Buzzega et al., 2020]. While we focussed on classification tasks in this work, GMC is based entirely on the idea of matching gradients and therefore directly applicable to other supervised learning tasks (e.g., regression) or unsupervised learning, e.g., with auto-encoders. Moreover, it would be interesting to make the coreset size *adaptive* by replacing the fixed subset size in OMP (Algorithm 1) with a threshold on the residual error. This would allow the algorithm to allocate additional memory resources in response to the “novelty” of the incoming data. Finally, it would be desirable to better understand the algorithm from a theoretical perspective, e.g., by strengthening the connection to the neural tangent kernel theory in the infinite width limit.

References

- Dimitris Achlioptas. Database-friendly random projections. In *Proceedings of the twentieth ACM SIGMOD-SIGACT-SIGART symposium on Principles of database systems*, pages 274–281, 2001.
- Rahaf Aljundi, Min Lin, Baptiste Goujaud, and Yoshua Bengio. Gradient based sample selection for online continual learning, 2019.
- Sanjeev Arora, Simon S Du, Wei Hu, Zhiyuan Li, Russ R Salakhutdinov, and Ruosong Wang. On exact computation with an infinitely wide neural net. In H. Wallach, H. Larochelle, A. Beygelzimer, F. d'Alché-Buc, E. Fox, and R. Garnett, editors, *Advances in Neural Information Processing Systems*, volume 32. Curran Associates, Inc., 2019. URL <https://proceedings.neurips.cc/paper/2019/file/dbc4d84bfcfe2284ba11beffb853a8c4-Paper.pdf>.
- Jordan T. Ash, Chicheng Zhang, Akshay Krishnamurthy, John Langford, and Alekh Agarwal. Deep batch active learning by diverse, uncertain gradient lower bounds. In *International Conference on Learning Representations*, 2020.
- Zalán Borsos, Mojmír Mutný, and Andreas Krause. Coresets via bilevel optimization for continual learning and streaming. *arXiv preprint arXiv:2006.03875*, 2020.
- Pietro Buzzega, Matteo Boschini, Angelo Porrello, Davide Abati, and Simone Calderara. Dark experience for general continual learning: a strong, simple baseline. *Advances in neural information processing systems*, 33:15920–15930, 2020.
- Trevor Campbell and Tamara Broderick. Bayesian coresets construction via greedy iterative geodesic ascent. In *International Conference on Machine Learning*, pages 698–706. PMLR, 2018.
- Arslan Chaudhry, Marcus Rohrbach, Mohamed Elhoseiny, Thalaiyasingam Ajanthan, Puneet K Dokania, Philip HS Torr, and Marc’Aurelio Ranzato. On tiny episodic memories in continual learning. *arXiv preprint arXiv:1902.10486*, 2019.
- Kaiming He, Xiangyu Zhang, Shaoqing Ren, and Jian Sun. Delving deep into rectifiers: Surpassing human-level performance on imagenet classification. In *Proceedings of the IEEE international conference on computer vision*, pages 1026–1034, 2015.
- Kaiming He, Xiangyu Zhang, Shaoqing Ren, and Jian Sun. Deep residual learning for image recognition. In *Proceedings of the IEEE conference on computer vision and pattern recognition*, pages 770–778, 2016.
- Jiayuan Huang, Arthur Gretton, Karsten Borgwardt, Bernhard Schölkopf, and Alex Smola. Correcting sample selection bias by unlabeled data. *Advances in neural information processing systems*, 19, 2006.
- Arthur Jacot, Franck Gabriel, and Clement Hongler. Neural tangent kernel: Convergence and generalization in neural networks. In S. Bengio, H. Wallach, H. Larochelle, K. Grauman, N. Cesa-Bianchi, and R. Garnett, editors, *Advances in Neural Information Processing Systems*, volume 31. Curran Associates, Inc., 2018. URL <https://proceedings.neurips.cc/paper/2018/file/5a4be1fa34e62bb8a6ec6b91d2462f5a-Paper.pdf>.
- Krishnateja Killamsetty, Durga Sivasubramanian, Baharan Mirzasoleiman, Ganesh Ramakrishnan, Abir De, and Rishabh Iyer. Grad-match: A gradient matching based data subset selection for efficient learning. *arXiv preprint arXiv:2103.00123*, 2021.
- Diederik P Kingma and Jimmy Ba. Adam: A method for stochastic optimization. *arXiv preprint arXiv:1412.6980*, 2014.
- James Kirkpatrick, Razvan Pascanu, Neil Rabinowitz, Joel Veness, Guillaume Desjardins, Andrei A Rusu, Kieran Milan, John Quan, Tiago Ramalho, Agnieszka Grabska-Barwinska, et al. Overcoming catastrophic forgetting in neural networks. *Proceedings of the national academy of sciences*, 114(13):3521–3526, 2017.
- Alex Krizhevsky, Geoffrey Hinton, et al. Learning multiple layers of features from tiny images. 2009.
- Yann LeCun and Corinna Cortes. MNIST handwritten digit database. 2010. URL <http://yann.lecun.com/exdb/mnist/>.
- Ping Li, Trevor J Hastie, and Kenneth W Church. Very sparse random projections. In *Proceedings of the 12th ACM SIGKDD international conference on Knowledge discovery and data mining*, pages 287–296, 2006.
- Zhizhong Li and Derek Hoiem. Learning without forgetting. *IEEE transactions on pattern analysis and machine intelligence*, 40(12):2935–2947, 2017.
- David Lopez-Paz and Marc’Aurelio Ranzato. Gradient episodic memory for continual learning. *Advances in neural information processing systems*, 30, 2017.
- Stéphane G Mallat and Zhifeng Zhang. Matching pursuits with time-frequency dictionaries. *IEEE Transactions on signal processing*, 41(12):3397–3415, 1993.
- Arun Mallya and Svetlana Lazebnik. Packnet: Adding multiple tasks to a single network by iterative pruning. In *Proceedings of the IEEE conference on Computer Vision and Pattern Recognition*, pages 7765–7773, 2018.

- Adam Paszke, Sam Gross, Francisco Massa, Adam Lerer, James Bradbury, Gregory Chanan, Trevor Killeen, Zeming Lin, Natalia Gimelshein, Luca Antiga, Alban Desmaison, Andreas Kopf, Edward Yang, Zachary DeVito, Martin Raison, Alykhan Tejani, Sasank Chilamkurthy, Benoit Steiner, Lu Fang, Junjie Bai, and Soumith Chintala. PyTorch: An imperative style, high-performance deep learning library. In H. Wallach, H. Larochelle, A. Beygelzimer, F. d'Alché-Buc, E. Fox, and R. Garnett, editors, *Advances in Neural Information Processing Systems 32*, pages 8024–8035. Curran Associates, Inc., 2019.
- Ameya Prabhu, Philip HS Torr, and Puneet K Dokania. Gdumb: A simple approach that questions our progress in continual learning. In *European conference on computer vision*, pages 524–540. Springer, 2020.
- Sylvestre-Alvise Rebuffi, Alexander Kolesnikov, Georg Sperl, and Christoph H Lampert. icarl: Incremental classifier and representation learning. In *Proceedings of the IEEE conference on Computer Vision and Pattern Recognition*, pages 2001–2010, 2017.
- Anthony Robins. Catastrophic forgetting, rehearsal and pseudorehearsal. *Connection Science*, 7(2):123–146, 1995.
- Ron Rubinstein, Michael Zibulevsky, and Michael Elad. Efficient implementation of the k-svd algorithm using batch orthogonal matching pursuit. Technical report, Computer Science Department, Technion, 2008.
- Andrei A Rusu, Neil C Rabinowitz, Guillaume Desjardins, Hubert Soyer, James Kirkpatrick, Koray Kavukcuoglu, Razvan Pascanu, and Raia Hadsell. Progressive neural networks. *arXiv preprint arXiv:1606.04671*, 2016.
- Joan Serra, Didac Suris, Marius Miron, and Alexandros Karatzoglou. Overcoming catastrophic forgetting with hard attention to the task. In *International Conference on Machine Learning*, pages 4548–4557. PMLR, 2018.
- Alex Smola, Arthur Gretton, Le Song, and Bernhard Schölkopf. A hilbert space embedding for distributions. In *International Conference on Algorithmic Learning Theory*, pages 13–31. Springer, 2007.
- Joaquin Vanschoren, Jan N. van Rijn, Bernd Bischl, and Luis Torgo. Openml: Networked science in machine learning. *SIGKDD Explorations*, 15(2):49–60, 2013. doi: 10.1145/2641190.2641198. URL <http://doi.acm.org/10.1145/2641190.2641198>.
- Jeffrey S Vitter. Random sampling with a reservoir. *ACM Transactions on Mathematical Software (TOMS)*, 11(1): 37–57, 1985.
- Han Xiao, Kashif Rasul, and Roland Vollgraf. Fashion-mnist: a novel image dataset for benchmarking machine learning algorithms, 2017.
- Mehrdad Yaghoobi, Di Wu, and Mike E Davies. Fast non-negative orthogonal matching pursuit. *IEEE Signal Processing Letters*, 22(9):1229–1233, 2015.
- Jaehong Yoon, Divyam Madaan, Eunho Yang, and Sung Ju Hwang. Online coreset selection for rehearsal-based continual learning. *arXiv preprint arXiv:2106.01085*, 2021.
- Friedemann Zenke, Ben Poole, and Surya Ganguli. Continual learning through synaptic intelligence. In *International Conference on Machine Learning*, pages 3987–3995. PMLR, 2017.
- Bo Zhao, Konda Reddy Mopuri, and Hakan Bilen. Dataset condensation with gradient matching. *arXiv preprint arXiv:2006.05929*, 2020.

A DETAILS ON GMC

This section provides a number of details on our gradient-matching coreset method that have been omitted from the main text.

A.1 SPARSE RANDOM PROJECTIONS

As mentioned in Section 2.1, we use dimensionality reduction on the gradient embeddings. Following Achlioptas [2001], we use sparse random projections with a density $\rho \in (0, 1]$. The elements of $P \in \mathbb{R}^{d \times D}$ are sampled as

$$P_{ij} = \begin{cases} -(\rho d)^{-1/2} & \text{with probability } \rho/2, \\ 0 & \text{with probability } 1 - \rho, \\ (\rho d)^{-1/2} & \text{with probability } \rho/2. \end{cases} \quad (15)$$

These projections satisfy $\mathbf{E}[P^T P] = I$ by construction and thereby preserve inner products in expectation. Since our algorithm is based entirely on inner products between gradient embeddings, this is a crucial property.

Following recommendations by Li et al. [2006], we set $\rho = 1/\sqrt{D}$ for a good trade-off between memory efficiency and reconstruction quality. This pushes the memory required to store P down to $O(d\sqrt{D})$. Note that it would be infeasible to store a dense $d \times D$ matrix for large model where D is in the tens of millions.

A.2 LAST-LAYER GRADIENTS

The gradients w.r.t. the last layer’s weights can be computed efficiently. We separate the forward map as $x \mapsto Wh(x; \theta)$, where $h(x; \theta)$ denotes the penultimate layer representation of data point x and $W \in \mathbb{R}^{C \times H}$ is the weight matrix of the output layer. Then the loss as a function of W takes the form

$$l(W; x, y) = l(Wh(x; \theta), y) \quad (16)$$

and the gradient w.r.t. W is

$$\nabla_W l(W; x, y) = \nabla l(Wh(x; \theta), y) h(x; \theta)^T, \quad (17)$$

where ∇l denotes the gradient of the loss function w.r.t. its first argument, the prediction.

Consider the case of cross-entropy loss, where the predictions take the form of logits, i.e., unnormalized log probabilities, and the label $y \in \mathbb{R}^C$ is encoded as a one-hot vector. The loss function may be written as

$$l(s, y) = - \sum_{c=1}^C y_c \log \rho(s)_c, \quad (18)$$

where ρ is the softmax function, i.e., $\rho(s)_c = s_c / (\sum_{c'} s_{c'})$. The gradient is

$$\nabla l(s, y) = y - \rho(s). \quad (19)$$

These gradients can be obtained efficiently at essentially the cost of a forward pass through the network. One simply has to intercept the penultimate layer representations $h(x; \theta)$ during the forward pass.

A.3 CHOLESKY-BASED OMP

In each iteration of OMP, we have to invert the matrix $G_I^T G_I$. This can be done efficiently by incrementally updating the Cholesky decomposition of this matrix [Rubinstein et al., 2008]. When adding an element to the coreset, $I = \tilde{I} \cup \{k\}$, we can split the matrix like

$$G_I^T G_I = \begin{bmatrix} G_{\tilde{I}}^T G_{\tilde{I}} & G_{\tilde{I}}^T g_k \\ g_k^T G_{\tilde{I}} & \|g_k\|^2 \end{bmatrix}. \quad (20)$$

For better readability, we abstract this to

$$A = \begin{bmatrix} \tilde{A} & v \\ v^T & c \end{bmatrix}, \quad \tilde{A} \in \mathbb{R}^{n \times n}, v \in \mathbb{R}^n, c \in \mathbb{R}. \quad (21)$$

If we know the Cholesky decomposition $\tilde{A} = \tilde{L}\tilde{L}^T$, it is easy to verify that the Cholesky decomposition of A is given by $A = LL^T$, where

$$L = \begin{bmatrix} \tilde{L} & 0 \\ w^T & \sqrt{c - \|w\|^2} \end{bmatrix}, \quad w = \tilde{L}^{-1}v. \quad (22)$$

To obtain w , we have to solve a linear system with a triangular matrix, which can be done in $O(n^2)$ time. Subsequently, $A^{-1}b$ can be solved as $(L^T)^{-1}(L^{-1}b)$ with two more triangular solves. Overall, this makes the effort for inverting $G_I^T G_I$ quadratic instead of cubic.

Regularization When adding a regularization term to the matching problem as described in Section 2.3, we will have to invert the matrix $G_I^T G_I + \lambda I$. It is straight-forward to extend the Cholesky-based implementation to this case. We now have a matrix of the form

$$A + \lambda I = \begin{bmatrix} \tilde{A} + \lambda I & v \\ v^T & c + \lambda \end{bmatrix}. \quad (23)$$

Assuming we know the Cholesky decomposition $\tilde{A} + \lambda I = \tilde{L}\tilde{L}^T$, we have $A + \lambda I = LL^T$, where

$$L = \begin{bmatrix} \tilde{L} & 0 \\ w^T & \sqrt{c + \lambda - \|w\|^2} \end{bmatrix}, \quad w = \tilde{L}^{-1}v. \quad (24)$$

A.4 LOCAL VARIANT OF GMC

We also experimented with a “local” variant of GMC, which we regard as a naive adaptation of the method of Killamsetty et al. [2021] to the continual learning setting. After finishing training for a task/batch, we compute gradient embeddings locally, using only the current iterate and run GMC with

these embeddings. Since this corresponds to $S = 1$, we use a larger projection dimension d to get the same gradient embedding dimension as before.

Since the gradient embedding function now *changes* over time, this requires changes in Continual GMC (Alg. 2). Instead of storing the gradient embedding matrix of the coreset for use in the next iteration, we need to recompute the embeddings in each iteration. Also, we can not update the target vector (Eq. (9)) and instead approximate it by summing the gradients in the current coreset and the new batch of data. Otherwise, the algorithm proceeds as before using these local gradient embeddings.

B EXPERIMENTAL DETAILS

B.1 CONTINUAL LEARNING SCENARIOS

As mentioned in the main text, the class-incremental scenario on FASHIONMNIST and CIFAR-10 is obtained by splitting the 10 classes of the dataset into 5 tasks, consisting of classes $\{0, 1\}, \{2, 3\}, \dots, \{8, 9\}$. The algorithm is evaluated on the entire test set.

For the rotated scenario on MNIST, we split the dataset randomly into four folds, then apply rotations of 0, 90, 180 and 270 degrees, respectively. This is done to both the training and the test set and the algorithm is evaluated on the entire test set.

The task-free scenario for the tabular datasets is generated by sorting the data points according to the value of a single feature. We arbitrarily chose the first feature. The resulting sequence is split into 10 batches of approximately equal size. Since the sequence changes smoothly, there is no notion of distinct tasks. Nevertheless, the sorting generates a non-trivial pattern in the relative frequencies of the classes across the 10 batches, see Fig. 5. The algorithm is evaluated on the entire test set.

For all datasets, we use the provided train/test split.

B.2 MODEL ARCHITECTURES

All experiments have been implemented using PyTorch [Paszke et al., 2019]. The initialization distribution is the standard scheme implemented in PyTorch, called `kaiming_uniform`, due to He et al. [2015].

MLP The MLP architecture consists of two fully-connected hidden layers with 128 units each and ReLU activation, followed by a fully-connected output layer.

CNN The CNN architecture consists of three convolutional layers with a receptive field of 5×5 pixels and 32, 32 and 64 filters, respectively. Each convolutional layer is

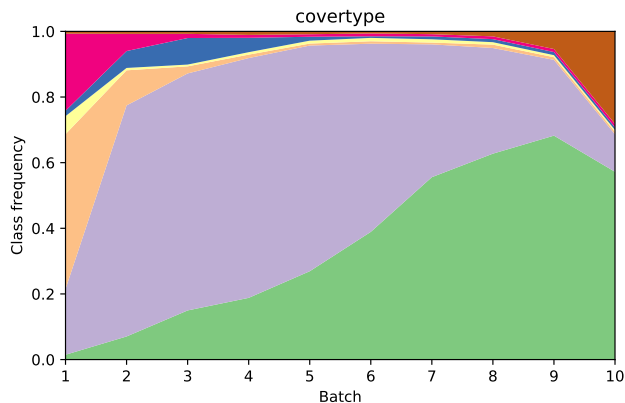


Figure 5: Class frequencies in the different batches of the task-free “sorted” scenario using the Coverttype dataset. Each color corresponds to one of the seven classes included in the dataset.

followed by max pooling over 2×2 windows and ReLU activation. This is followed by a fully-connected layer of 256 units with ReLU activation and a fully-connected output layer.

ResNet-18 as described by He et al. [2016] and implemented in the `torchvision` Python package.

B.3 OPTIMIZATION HYPERPARAMETERS

All models are trained using the Adam optimizer with a step size of $3 \cdot 10^{-4}$, a weight decay of 10^{-4} and default choices for the other hyperparameters. We use a minibatch size of 100. We train each model for a fixed number of 200 epochs, irrespective of the memory size and algorithm.

C ADDITIONAL RESULTS

C.1 FULL RESULTS

Tables 1 and 2 display the full results for all tested memory curation strategies using GDumb and ER, respectively. Missing entries for the GSS method correspond to training runs that time out.

C.2 CONTINUAL PERFORMANCE

The plots in the main text depict the performance after processing all tasks. To get a more fine-grained view of the continual behavior, Figures 6 and ?? depict the performance after each individual task. It shows results from the same experiments as in the main text, but zooms in on a single memory size of 500.

Table 1: Results in the GDumb setting. Final test accuracy [%] after seeing all tasks for different memory sizes.

	Coverttype				
	200	500	1000	2000	5000
GSS	30.74 ± 1.59	30.79 ± 2.63	34.38 ± 1.86	39.38 ± 1.16	-
GradientMatchingCoreset	66.07 ± 0.22	69.04 ± 0.22	70.64 ± 0.08	72.13 ± 0.34	74.18 ± 0.08
GreedyClassBalancing	4.99 ± 1.06	5.84 ± 1.01	7.42 ± 0.24	12.04 ± 0.46	19.75 ± 0.16
LastLayerGradientMatchingCoreset	66.07 ± 0.64	68.29 ± 0.40	69.65 ± 0.25	71.35 ± 0.41	73.84 ± 0.23
LocalGradientMatchingCoreset	64.01 ± 0.49	66.98 ± 0.38	68.95 ± 0.20	70.88 ± 0.39	73.52 ± 0.21
Reservoir	62.27 ± 0.58	64.03 ± 0.78	65.78 ± 1.44	68.46 ± 0.43	72.41 ± 0.51
SlidingWindow	18.23 ± 0.41	20.97 ± 1.03	21.18 ± 1.85	29.98 ± 0.94	57.60 ± 1.81
	LDPA				
	200	500	1000	2000	5000
GSS	23.09 ± 3.91	21.45 ± 2.42	21.91 ± 2.07	14.16 ± 0.44	16.61 ± 0.49
GradientMatchingCoreset	49.21 ± 0.43	54.15 ± 0.52	58.22 ± 0.32	61.55 ± 0.43	65.14 ± 0.29
GreedyClassBalancing	14.99 ± 1.59	10.82 ± 1.97	4.17 ± 0.37	5.44 ± 0.14	10.29 ± 0.28
LastLayerGradientMatchingCoreset	49.21 ± 0.30	53.17 ± 0.40	57.90 ± 0.52	61.08 ± 0.17	64.56 ± 0.20
LocalGradientMatchingCoreset	48.07 ± 0.28	51.11 ± 0.61	55.96 ± 0.48	59.35 ± 0.36	63.28 ± 0.38
Reservoir	44.83 ± 2.04	49.98 ± 0.76	54.46 ± 0.89	59.34 ± 0.42	64.17 ± 0.29
SlidingWindow	16.96 ± 0.77	15.76 ± 0.52	27.71 ± 1.29	32.63 ± 1.10	41.89 ± 1.91
	Walking Activity				
	200	500	1000	2000	5000
GSS	14.13 ± 1.29	18.13 ± 1.86	20.35 ± 2.39	15.51 ± 1.85	15.75 ± 2.33
GradientMatchingCoreset	37.97 ± 0.83	43.21 ± 0.18	45.67 ± 0.12	47.94 ± 0.39	51.51 ± 0.20
GreedyClassBalancing	13.46 ± 0.42	14.27 ± 1.73	19.93 ± 1.59	19.48 ± 0.34	21.22 ± 0.60
LastLayerGradientMatchingCoreset	37.25 ± 0.23	43.29 ± 0.12	45.84 ± 0.24	48.19 ± 0.20	51.46 ± 0.15
LocalGradientMatchingCoreset	36.13 ± 0.39	39.78 ± 0.31	43.17 ± 0.13	45.90 ± 0.16	49.73 ± 0.17
Reservoir	34.90 ± 1.08	40.33 ± 0.59	43.09 ± 0.69	46.50 ± 0.13	50.22 ± 0.17
SlidingWindow	14.73 ± 0.00	14.73 ± 0.00	17.40 ± 0.27	17.37 ± 0.27	16.82 ± 0.13
	MNIST				
	200	500	1000	2000	5000
GradientMatchingCoreset	63.75 ± 1.03	75.16 ± 0.73	81.72 ± 0.63	87.18 ± 0.25	92.82 ± 0.41
GreedyClassBalancing	35.09 ± 1.53	37.08 ± 0.65	38.34 ± 1.29	41.42 ± 0.93	63.38 ± 0.67
LastLayerGradientMatchingCoreset	65.63 ± 0.81	77.01 ± 0.93	83.37 ± 0.40	88.01 ± 0.30	93.22 ± 0.18
LocalGradientMatchingCoreset	58.97 ± 1.06	69.92 ± 0.43	76.61 ± 0.49	82.38 ± 0.26	88.87 ± 0.58
Reservoir	57.43 ± 0.96	73.92 ± 1.62	81.54 ± 0.53	86.56 ± 0.32	92.74 ± 0.35
SlidingWindow	34.57 ± 1.48	36.36 ± 0.27	38.34 ± 1.21	39.38 ± 1.00	42.56 ± 1.26
	FashionMNIST				
	200	500	1000	2000	5000
GradientMatchingCoreset	72.76 ± 0.97	78.15 ± 0.59	80.39 ± 0.89	83.16 ± 0.37	85.77 ± 0.18
GreedyClassBalancing	69.94 ± 0.66	75.63 ± 0.85	79.74 ± 0.67	82.79 ± 0.59	85.97 ± 0.36
LastLayerGradientMatchingCoreset	72.93 ± 0.55	78.93 ± 0.65	81.74 ± 0.34	83.98 ± 0.27	86.53 ± 0.27
LocalGradientMatchingCoreset	69.04 ± 0.90	75.10 ± 1.33	79.10 ± 1.18	82.46 ± 0.34	85.47 ± 0.24
Reservoir	68.59 ± 0.69	75.92 ± 0.88	79.57 ± 0.42	82.93 ± 0.21	85.78 ± 0.39
SlidingWindow	19.85 ± 0.03	19.91 ± 0.01	19.91 ± 0.01	19.92 ± 0.04	19.96 ± 0.01
	CIFAR-10				
	200	500	1000	2000	5000
GradientMatchingCoreset	14.19 ± 4.53	25.62 ± 0.53	27.34 ± 1.42	31.31 ± 0.43	35.46 ± 1.00
GreedyClassBalancing	16.44 ± 4.32	24.38 ± 0.73	26.01 ± 0.52	29.54 ± 0.66	34.43 ± 0.59
LastLayerGradientMatchingCoreset	12.12 ± 3.58	24.52 ± 0.80	26.25 ± 0.58	29.92 ± 1.59	34.71 ± 1.03
LocalGradientMatchingCoreset	18.06 ± 4.94	25.81 ± 1.06	27.76 ± 1.38	31.80 ± 0.88	35.45 ± 1.08
Reservoir	14.81 ± 4.40	24.70 ± 0.12	25.56 ± 0.97	29.46 ± 0.47	34.12 ± 0.68
SlidingWindow	11.28 ± 1.78	15.77 ± 0.25	15.92 ± 0.32	16.42 ± 0.07	16.87 ± 0.10

Table 2: Experimental results in the experience replay setting. Table shows final test accuracy [%] after seeing all tasks/batches for different memory sizes.

Coverttype					
	200	500	1000	2000	5000
GSS	58.99 ± 1.39	58.06 ± 1.57	57.02 ± 1.19	56.97 ± 2.10	-
GradientMatchingCoreset	66.33 ± 0.49	68.44 ± 0.74	70.83 ± 0.37	72.45 ± 0.36	75.30 ± 0.36
GreedyClassBalancing	36.00 ± 3.30	17.08 ± 1.46	17.12 ± 0.18	20.17 ± 0.25	26.82 ± 0.33
LastLayerGradientMatchingCoreset	65.72 ± 0.13	66.29 ± 0.87	68.42 ± 0.40	71.14 ± 0.50	74.20 ± 0.26
LocalGradientMatchingCoreset	52.16 ± 5.89	55.81 ± 2.52	51.82 ± 4.64	51.82 ± 1.04	59.93 ± 1.86
Reservoir	64.58 ± 0.62	66.58 ± 0.83	68.19 ± 0.72	70.48 ± 0.29	73.57 ± 0.35
SlidingWindow	57.10 ± 1.63	57.12 ± 1.45	59.10 ± 0.88	58.12 ± 0.86	49.94 ± 1.86
LDPA					
	200	500	1000	2000	5000
GSS	43.03 ± 2.40	38.65 ± 2.20	36.82 ± 1.02	39.23 ± 0.47	47.56 ± 1.27
GradientMatchingCoreset	53.42 ± 0.68	58.61 ± 0.41	62.10 ± 0.44	64.49 ± 0.24	66.75 ± 0.28
GreedyClassBalancing	37.83 ± 1.29	30.16 ± 2.23	14.75 ± 1.24	14.19 ± 0.48	17.78 ± 0.20
LastLayerGradientMatchingCoreset	51.67 ± 0.80	57.22 ± 0.49	61.08 ± 0.30	63.93 ± 0.28	66.36 ± 0.19
LocalGradientMatchingCoreset	33.00 ± 3.05	31.41 ± 4.89	39.71 ± 1.42	44.85 ± 2.66	50.29 ± 2.99
Reservoir	51.79 ± 1.00	56.33 ± 0.43	59.76 ± 0.51	62.38 ± 0.23	65.74 ± 0.27
SlidingWindow	40.96 ± 1.80	42.94 ± 1.61	43.79 ± 1.64	40.90 ± 1.29	43.23 ± 0.40
Walking Activity					
	200	500	1000	2000	5000
GSS	18.81 ± 0.52	16.94 ± 0.74	17.84 ± 0.61	22.54 ± 0.71	27.26 ± 0.49
GradientMatchingCoreset	40.16 ± 0.50	46.50 ± 0.74	49.24 ± 0.39	51.02 ± 0.27	53.60 ± 0.39
GreedyClassBalancing	20.69 ± 1.25	20.17 ± 1.21	22.73 ± 0.66	23.82 ± 0.41	27.52 ± 0.43
LastLayerGradientMatchingCoreset	38.17 ± 1.79	46.59 ± 0.57	49.17 ± 0.31	50.99 ± 0.26	53.47 ± 0.17
LocalGradientMatchingCoreset	24.17 ± 2.80	32.56 ± 2.56	38.28 ± 1.36	41.72 ± 1.25	45.51 ± 1.04
Reservoir	38.18 ± 1.10	43.11 ± 0.33	45.39 ± 0.57	48.54 ± 0.22	51.99 ± 0.20
SlidingWindow	21.02 ± 0.42	21.80 ± 0.60	20.92 ± 0.98	21.81 ± 0.37	22.17 ± 0.21
MNIST					
	200	500	1000	2000	5000
GSS	63.04 ± 1.22	65.02 ± 0.39	66.36 ± 0.76	67.05 ± 0.43	67.42 ± 0.51
GradientMatchingCoreset	80.80 ± 0.41	87.93 ± 0.80	91.39 ± 0.47	94.02 ± 0.12	95.47 ± 1.05
GreedyClassBalancing	63.11 ± 0.75	64.77 ± 0.20	66.08 ± 0.77	66.93 ± 0.44	79.38 ± 0.74
LastLayerGradientMatchingCoreset	81.51 ± 0.94	88.84 ± 0.38	92.11 ± 0.35	93.96 ± 0.44	96.27 ± 0.13
LocalGradientMatchingCoreset	52.53 ± 1.40	62.20 ± 2.63	71.88 ± 3.15	82.88 ± 1.35	86.72 ± 4.52
Reservoir	72.93 ± 1.96	82.01 ± 2.02	88.85 ± 0.53	92.96 ± 0.45	95.67 ± 0.12
SlidingWindow	62.13 ± 0.92	65.36 ± 0.52	66.04 ± 0.97	66.82 ± 0.43	67.72 ± 0.54
FashionMNIST					
	200	500	1000	2000	5000
GSS	-	-	39.00 ± 0.00	39.42 ± 0.01	-
GradientMatchingCoreset	71.67 ± 1.06	78.16 ± 0.66	81.61 ± 0.64	84.33 ± 0.41	87.20 ± 0.26
GreedyClassBalancing	67.03 ± 0.65	74.86 ± 1.08	79.35 ± 0.81	83.30 ± 0.37	86.55 ± 0.30
LastLayerGradientMatchingCoreset	72.52 ± 0.26	77.95 ± 0.84	81.92 ± 0.36	84.56 ± 0.48	87.53 ± 0.33
LocalGradientMatchingCoreset	28.93 ± 2.68	39.47 ± 6.36	46.93 ± 4.47	53.36 ± 4.11	59.55 ± 3.13
Reservoir	67.78 ± 1.12	74.34 ± 2.80	78.84 ± 0.82	82.89 ± 1.57	86.38 ± 0.27
SlidingWindow	35.17 ± 0.21	36.82 ± 0.15	37.91 ± 0.14	38.61 ± 0.07	39.00 ± 0.13
CIFAR-10					
	200	500	1000	2000	5000
GradientMatchingCoreset	24.35 ± 0.92	27.47 ± 2.13	30.33 ± 1.37	33.83 ± 0.94	39.38 ± 0.93
GreedyClassBalancing	19.44 ± 2.00	22.71 ± 0.90	28.29 ± 0.89	30.89 ± 0.56	36.90 ± 0.61
LastLayerGradientMatchingCoreset	18.54 ± 1.96	23.09 ± 2.24	25.34 ± 1.47	29.27 ± 0.99	36.50 ± 0.29
LocalGradientMatchingCoreset	21.62 ± 1.23	23.22 ± 1.43	24.96 ± 1.54	27.65 ± 0.60	30.99 ± 0.63
Reservoir	19.15 ± 1.32	23.18 ± 1.45	27.24 ± 0.66	31.13 ± 1.47	37.70 ± 0.56
SlidingWindow	20.73 ± 1.19	24.18 ± 0.78	26.65 ± 0.38	27.91 ± 0.61	30.56 ± 0.26

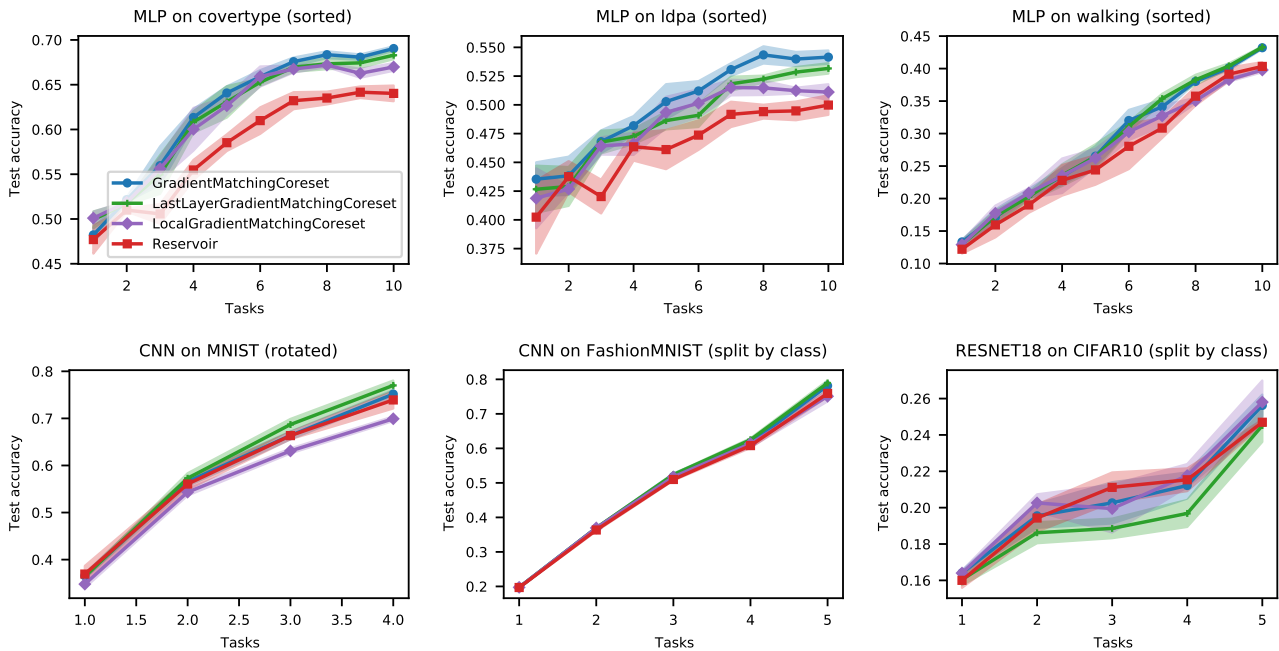


Figure 6: Results on continual learning scenarios using the GDumb paradigm with different subsampling/coreset methods at a memory size of 500. The graphs depict the accuracy on the full test set after the processing of each task/batch. Results are averaged over five random seeds and the shaded area spans one standard deviation.

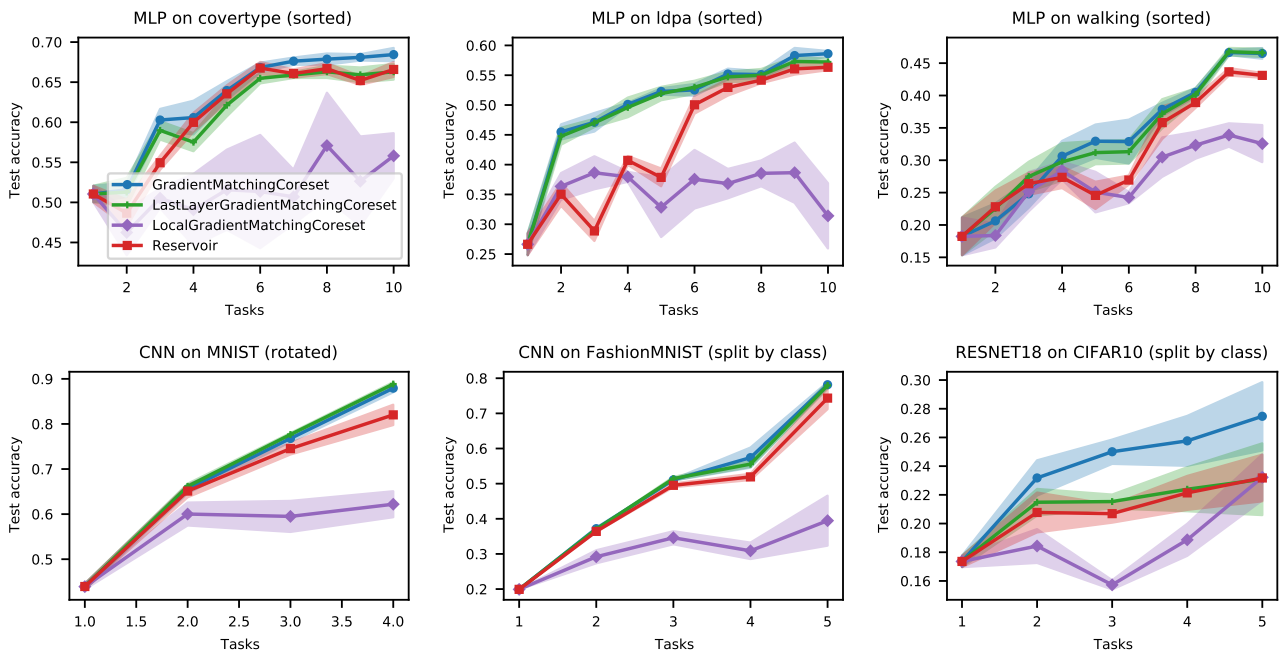


Figure 7: Results on continual learning scenarios using the Experience Replay paradigm with different subsampling/coreset methods at a memory size of 500. The graphs depict the accuracy on the full test set after the processing of each task/batch. Results are averaged over five random seeds and the shaded area spans one standard deviation.

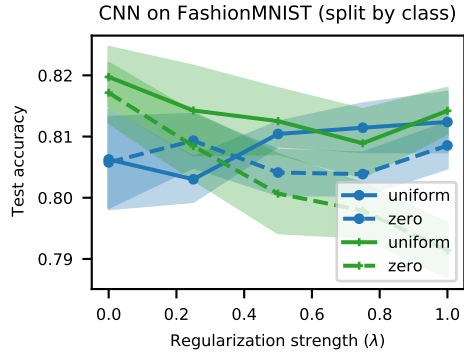


Figure 8: Comparing regularization schemes.

C.3 ADDITIONAL ABLATIONS

Regularization strategy In Section 2.3, we proposed a regularization scheme that regularizes OMP towards a uniform solution. In this ablation study, we compare this to a simple zero-centered regularization term as used by Kilamsetty et al. [2021]. Results are depicted in Fig. 8. While the differences are not enormous, the zero-centered regularizer performs slightly worse. We also observed that zero-centered regularization led to (a small number) of coreset elements being assigned a negative weight and therefore being effectively removed by clipping the weights at zero.